

# High-refractive-index tin sulfide core-shell spheres for photonic applications

X. T. Peng<sup>1,2</sup> and A. D. Dinsmore<sup>1\*</sup>

<sup>1</sup>*Department of Physics, University of Massachusetts Amherst, 01003 USA*

<sup>2</sup>*Current address: Alliance Fiber Optics Products, Inc., Sunnyvale CA 94089*

\*Address correspondence to this author. E-mail: dinsmore@physics.umass.edu

We describe the fabrication of core-shell colloidal spheres composed of a shell of tin sulfide and a core of polystyrene. The tin sulfide shell is deposited on micron-sized latex spheres using a sonochemical technique. By angle-dependent light scattering and electron microscopy, we find that the refractive index of the shell is 3.0 at a wavelength of 1064 nm and the shell's thickness is controllable in the range of 30-60 nm. The resulting spheres have a narrow distribution of sizes, are stable in aqueous suspension, and are very strong scatterers in the near-infrared with potential application in photonic band-gap materials or other photonic devices.

Keywords: colloid, optical properties, core/shell

## I. INTRODUCTION

In the approximately twenty years since the concepts of strong localization and the photonic band gap were developed, a great deal of research has gone into the practical problem of achieving the desired structure and sufficiently large variation in the refractive index.<sup>1-8</sup> In the visible to near-infrared range, much of the fabrication effort has focused on either lithography from a solid substrate or self-assembly of colloidal particles. The latter potentially offers advantages of low cost and scalability and might lead to three-dimensional structures, either crystalline or random, that are not readily achieved by lithography. A major challenge of the self-assembly route, however, is achieving a large refractive index  $n$ , since the materials that are amenable to handling in suspension often have low intrinsic refractive index or are porous. Constructing a material with a full photonic band gap requires  $n > 2$  (if the diamond lattice can be achieved)<sup>9</sup> or  $n > 2.6$  (for the more readily formed face-centered cubic lattice).<sup>10,11</sup> Large  $n$  has been achieved by infiltration of a pre-assembled colloidal crystal by chemical precursors to form TiO<sub>2</sub>,<sup>12</sup> carbon,<sup>13</sup> silicon,<sup>14</sup> or SnS<sub>2</sub>.<sup>15</sup> To form ordered structures or for application as tracers or pigments in paints, it is desirable to have controlled morphology and a narrow distribution of sizes. Moreover, particles with a core-shell morphology are also promising because they can be assembled in close-packed lattices that provide an optimal volume fraction of high- $n$  material (on the order of 25 vol%).<sup>16-18</sup> To date, uniform core-shell particles with a narrow distribution of sizes have been made with ZnS core and low- $n$  silica shell,<sup>19</sup> or with a polymeric or silica core and a high- $n$  shell of ZnS,<sup>20-26</sup> ZnSe,<sup>27</sup> ZnO,<sup>28</sup> or TiO<sub>2</sub>.<sup>29,30</sup> The effective refractive index of the high- $n$  material is typically inferred rather than measured, and its value is typically lower than the intrinsic material because of porosity. It is therefore important to include in the materials analysis a measurement of the optical properties of the individual particles.

Here we describe sonochemical synthesis and characterization of colloidal spheres having a polystyrene core and a uniform and high- $n$  shell of tin sulfide. Tin sulfide has a

very large refractive index and is transparent in the near infrared, either in the form of SnS<sub>2</sub> ( $n \approx 3.0$  for  $\lambda \sim 1 \mu\text{m}$ )<sup>15,31-33</sup> or SnS ( $n \geq 4.1$  for  $\lambda \sim 1 \mu\text{m}$ ),<sup>34</sup> these compounds are therefore attractive for the applications described above. Synthesis by sonochemistry is a very flexible technique that has been reviewed extensively.<sup>35</sup> For example, this method was used previously to form polystyrene-ZnS core-shell spheres where the shell had  $n$  approximately 2.<sup>20</sup>

We report angle-dependent light scattering data showing that the real part of the refractive index of the tin sulfide shell is  $n = 3.0$  at wavelength  $\lambda = 1064 \text{ nm}$ . The imaginary part, arising from optical absorption, is 0.6. The core-shell spheres have a narrow distribution of sizes and are stable in suspension. The thickness of the tin sulfide shell can be varied between approximately 30 and 60 nm, though the shell morphology becomes irregular for thicker layers. The combination of colloidal stability and uniformity with low- $n$  core and high- $n$  shell makes these promising materials as tracer particles in scattering experiments or for future studies of strong localization of light and photonic band gaps.

## II. EXPERIMENTAL METHODS

**Sonochemical Synthesis.** The tin sulfide precipitation was carried out in aqueous solution with the colloidal spheres. Tin (II) chloride (98+ % purity) and thioacetamide (TAA, 99+ % purity) were purchased (Aldrich, Milwaukee, WI) and used without further purification. We began by mixing SnCl<sub>2</sub> and 50 mL of filtered water (Milli-Q; Millipore Corp., Billerica, MA) in a 50-mL round-bottom flask. The solution was agitated in a sonic bath for 30 s or until all of the metal salt dissolved. We then added 1 mL of 5 wt% carboxylate-modified polystyrene (PS-CO<sub>2</sub>) microspheres. The microspheres were used as received from Seradyn Inc. (Indianapolis, IN) or Interfacial Dynamics Corporation (Eugene, OR). Proprietary surfactant that might be in solution with the microspheres was found not to interfere with deposition. TAA was then added. Various concentrations of SnCl<sub>2</sub> and TAA were used, but always with a 2:1 molar ratio with typical amounts being 310 mg or (0.033 M) of SnCl<sub>2</sub> and 246 mg (0.066 M) of TAA.

A 750-Watt, 20-kHz ultrasonic processor (Ace Glass, Vineland, NJ) was used to initiate the reaction. Ultrasonic irradiation was delivered by a 0.25-inch-diameter titanium, tapered micro-tip probe. The sonic probe was immersed in the reaction solution and the power was pulsed (0.5/0.5 s on/off) for up to 6 hours at 20% of the total power (*i.e.*, 150 W). To monitor film growth over time, aliquots of the reaction solution (0.50 mL each) were collected prior to sonication, and then subsequently at intervals of approximately 40 min. The final product was washed several times with Milli-Q-filtered water.

**Scanning and Transmission Electron Microscopy (SEM and TEM).** Particles were dried onto a TEM grid for visualization of the core-shell morphology (JEOL 100CX, 100 kV). To visualize the surface morphology, the tin sulfide core-shell particles were also imaged with a scanning electron microscope after coating with a thin layer of gold (JEOL JSM-6400).

**X-ray Diffraction.** The tin sulfide core-shell particles were dried onto a silicon wafer for x-ray diffraction (XRD). We used a Rigaku diffractometer with Cu K<sub>α</sub> x-rays having a wavelength of 1.54 Å.

**Light Scattering.** We used static light scattering (wavelength: 1064 nm) from a dilute suspension to measure the refractive index of the tin sulfide shell. For the light-

scattering measurements, particles were suspended in cyclohexane ( $n \sim 1.425$ ) to reduce the total scattering and thereby suppress multiple scattering of light. To prevent the tin-sulfide-coated spheres from aggregating in the cyclohexane, we added the surfactant dioctyl sulfosuccinate sodium salt (AOT, 99%; Aldrich, Milwaukee WI) to achieve a concentration of 0.5-1%.

A dilute suspension was placed in a small glass vial, which was itself placed in a larger glass vial filled with cyclohexane. The refractive index of cyclohexane matches that of the glass reasonably well, which minimizes reflections. Stray scattered light (*e.g.*, from glass/air interface) was carefully blocked with beam absorbers and apertures. The glass vials were placed at the center of a goniometer. Laser radiation with wavelength  $\lambda$  of 1064 nm was used to illuminate the sample solution. The scattered intensity from the sample was collected with a silicon photodiode (Thorlabs, Inc., Newton NJ), which was scanned across a range of angles, approximately from 10-130°. The goniometer and the photodiode signal acquisition were controlled using LabVIEW (National Instruments, Austin TX).

The suspension was sufficiently dilute to avoid multiple scattering of light and to avoid structural correlations of the scattering spheres. The intensity from a cell filled only with cyclohexane was subtracted from the data. The result is proportional to the differential cross section  $d\sigma/d\theta$  of isolated spheres in the solvent. As described below, we used Mie scattering theory to fit to the measured cross section and obtain the dimensions and refractive indices of the particles.

### III. RESULTS AND DISCUSSION

Electron microscopy images (Fig. 1) show a smooth tin sulfide shell with thickness ranging from 30nm-60nm. Figure 1(a) shows a TEM image of 0.97- $\mu\text{m}$ -diameter PS spheres formed in a reaction with 0.033 M  $\text{SnCl}_2$ , 0.066 M TAA, and reaction time of 3 h. The higher atomic number of tin leads to the contrast in the image and shows that the tin sulfide forms a shell at the surface. Images of the PS spheres prior to the reaction show only the gray interior regions with no dark shell (images not shown). Figure 1(b) shows a scanning-electron microscope image of spheres coated with the same reaction conditions, but after 90 min of reaction time. Both SEM and TEM show smooth, spherical particles.

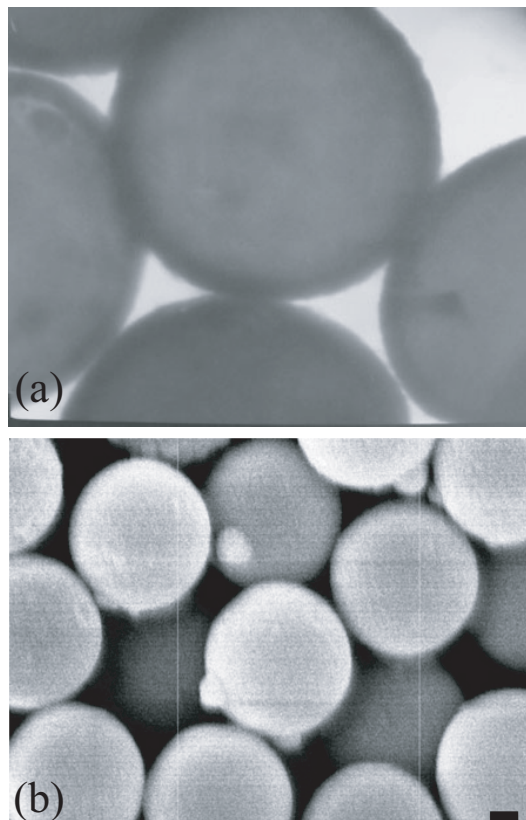


FIG. 1. Electron microscope images of tin-sulfide-coated polystyrene spheres. (a) TEM image, where the tin sulfide appears as a dark ring around the polystyrene. The polystyrene-core diameter is 0.97  $\mu\text{m}$ . (b) SEM image; scale bar represents 0.2  $\mu\text{m}$ .

The particles have a sufficiently narrow distribution of sizes so that they can form ordered structures, as shown in Fig. 2. These structures were formed in aqueous suspension in the presence of an AC electric field (40 kHz, 10 V across approximately 0.8 cm). Single-layer (Fig 2a) and multi-layer (Fig. 2b) structures were formed. In the multi-layer structures, only the surface layer was visible owing to the strong scattering of light by the high- $n$  shell.

Figure 3(a) shows the thickness of the tin sulfide shell as a function of the duration of the sonication reaction. The reaction conditions were the same as for the particles of Fig. 1 (0.033 M  $\text{SnCl}_2$  and 0.066 M TAA, and 0.97  $\mu\text{m}$ -diameter PS spheres). The thickness was measured from TEM images. The data are in close agreement with an exponential growth curve having a characteristic ( $1/e$ ) time of 90 min. After three hours, the growth had effectively stopped at a terminal shell thickness of 60 nm. The terminal thickness depends linearly on the concentration of TAA and  $\text{SnCl}_2$ , as shown in Fig. 3(b). In these experiments, the initial molar ratio of  $\text{SnCl}_2$ :TAA was held at 2:1, but the total initial concentration was varied. The data agree well with a linear fit with slope of 870 nm per M of TAA. The surface becomes rougher, however, when the shell thickness exceeds approximately 60 nm and some images showed small bumps of tin sulfide clusters on top of the shell. These clusters were rarely found in the formation of ZnS shells on PS spheres by a similar technique,<sup>20</sup> which we repeated in our lab for comparison. We speculate that the small clusters formed here because the  $\text{SnCl}_2$  only partially dissolved in solution, and might therefore have created nucleation centers for the small clusters. By contrast, the zinc precursor ( $\text{Zn}(\text{Ac})_2$ ) completely dissolved in solution and the nucleation might have been restricted to the particles' surfaces.

The x-ray diffraction (XRD) spectrum, shown in Fig. 4, provides some insight into the structure and composition of the shell. This sample was made under the same conditions as those of Fig. 1(b) (reaction time of 90 min). The spectrum shows a pronounced peak at approximately  $29^\circ$  and perhaps a weak secondary peak near  $52^\circ$ , both of which we attribute to the tin sulfide shell. The main peak was substantially broadened by the small size of the crystallites. We extract the average crystallite size ( $t$ ) from the full width at half maximum ( $\Delta$ ) of the diffraction peak using Scherrer's formula:  $t = K \lambda / [\Delta * \cos(\theta_p)]$ .<sup>36</sup> Here,  $K$  is the Scherrer constant, whose value falls in the range 0.87-1.0 (we assume the value of 0.9 as is commonly done);  $\lambda$  is the x-ray wavelength (1.54  $\text{\AA}$ );  $\theta_p$  is the peak position. This analysis yields an estimated average crystallite size of 2.1 nm. This small particulate size is consistent with the smooth appearance seen in SEM and TEM.

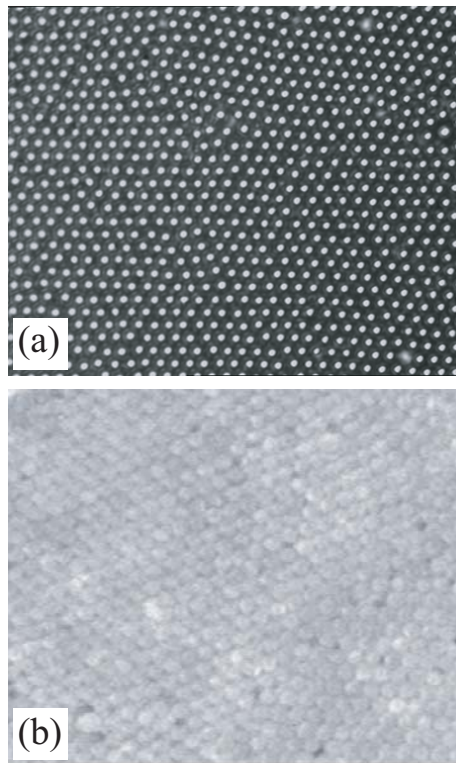


FIG. 2. (a) Optical image of a layer of tin-sulfide-coated polystyrene spheres assembled on the surface of a glass coverslip. (b) Optical image of a multi-layer, polycrystalline structure. The particle diameter is approximately 1  $\mu\text{m}$ .

To identify the material of the shell, we compare our spectrum to previously reported XRD patterns from hexagonal SnS<sub>2</sub> and two different symmetries of SnS (orthorhombic and zincblende).<sup>37,38</sup> Chen *et al* used a microwave-assisted process starting with thiourea and tin chloride precursors in ethylene glycol, with SnCl<sub>2</sub> leading to orthorhombic SnS and SnCl<sub>4</sub> leading to hexagonal SnS<sub>2</sub>. The large width of the main peak in our results (arising from the small domain size) makes an exact determination of the structure difficult. Nonetheless, the position of the main peak corresponds fairly closely to the strongest (100) peak of hexagonal SnS<sub>2</sub>, with perhaps some contribution from the weaker and broader (101) peak. It seems surprising, however, that using SnCl<sub>2</sub> as a precursor would lead to SnS<sub>2</sub> rather than SnS (which is in contrast to the results of the previous microwave-assisted process<sup>37</sup>). An alternative explanation is that the shell material is the zincblende structure of SnS, as reported previously from thermal decomposition of SnCl<sub>2</sub> and elemental S.<sup>39</sup> The predominant (111) and (200) peaks of this zincblende structure appear at angles of approximately 26 and 31°,<sup>39,40</sup> close to the angle where we find our major peak. As we discuss below, the optical measurements of the refractive index are more consistent with the SnS structure.

The light-scattering data for the tin sulfide core-shell spheres suspended in cyclohexane are shown in Fig. 5. Multiple measurements were made using multiple samples, and consistent results were obtained. In brief, our method of analysis is to perform a fit of the measured scattering intensity *vs.* angle to calculated differential cross section of the core-shell particles,  $d\sigma/d\theta$ . Since  $d\sigma/d\theta$  is a nontrivial function of sizes and refractive indices, we used the simplex fitting method with an algorithm known as amoeba,<sup>41</sup> which was implemented in IDL (ITT Visual Information Solutions, Boulder, CO). The values of  $d\sigma/d\theta$  were computed using the numerical routine known as “bhcoat,” written in FORTRAN by Bohren and Huffman,<sup>42</sup> which we implemented in IDL. To carry out the fit, we used eight adjustable parameters, of which five can be compared to known values to help assess the quality of the fit. Five of the fit parameters are the refractive indices of the solvent ( $n_0$ ), of the core ( $n_c$ ), and of the shell ( $n_s$ ). The latter two are complex numbers, reflecting the presence

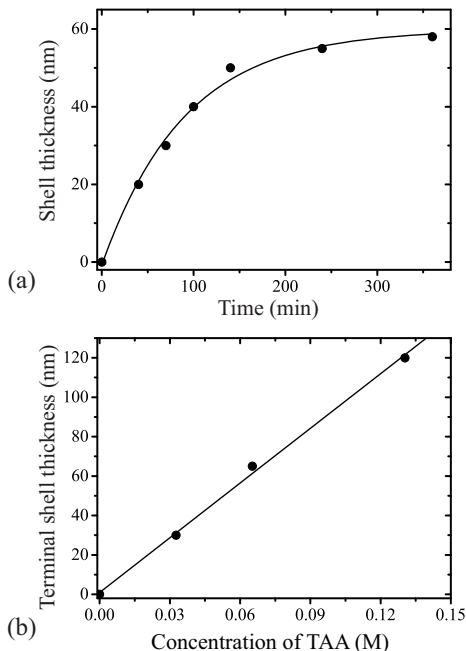


FIG. 3. Thickness of the tin sulfide shell, as measured by TEM. (a) Thickness *vs.* time for 0.033 M SnCl<sub>2</sub>, 0.066 M TAA, and 0.97 μm-diameter PS spheres. The curve shows a fit to an exponential growth. (b) The terminal (long-time) thickness as a function of concentration of thioacetamide (TAA), showing a linear dependence.

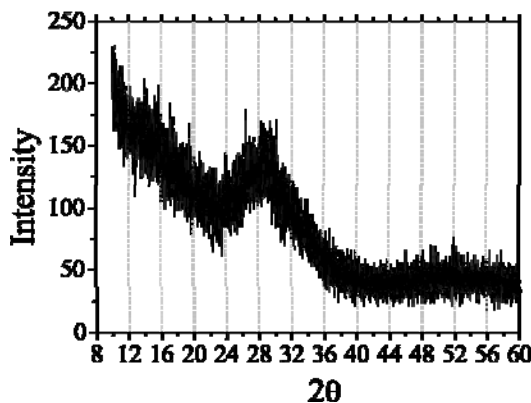


FIG. 4. The measured x-ray diffraction (XRD) intensity as a function of scattering angle for the core-shell spheres.

of absorption; they therefore each contain both real and imaginary parts. The core radius ( $R_c$ ), shell radius ( $R_s$ ), and an arbitrary overall coefficient (related to concentration and detection efficiency) are the remaining fit parameters. The best fit was obtained with  $n_s = 3.015 + 0.638i$ . We also obtained  $n_0 = 1.427$ , which compares well to the value of 1.425 measured using a visible-light refractometer. For the polystyrene core, we found  $n_c = 1.52 + 0.168i$ . Previous measurements at this wavelength (1064 nm) yielded a refractive index of polystyrene equal to  $1.575 + 0.001i$ ;<sup>43</sup> the small difference might be due to penetration of solvent or reactant

into our polystyrene spheres. We further found  $R_c = 500.1$  nm and a shell thickness of 34.4 nm, both of which agree with our electron microscopy measurements within error. Since we know that the polystyrene spheres have a polydispersity of radius, we then computed the average  $d\sigma/d\theta$  for an approximately Gaussian distribution of  $R_c$  values with a standard deviation of 1% (which is the manufacturer's reported size polydispersity for the starting latex suspension). The result of this calculation agrees quite well with the experimental data, as shown in the plot of Fig. 5. We regard the agreement is satisfactory though still not perfect. The remaining differences might arise from a gradient in refractive index near the polystyrene-tin sulfide boundary, and some roughness and/or polydispersity of the shell thickness. We note, however, that increasing or decreasing the refractive index of the shell leads to an inferior agreement of data and fitted curve. The inset of Fig. 5 shows the values of  $\chi^2$  obtained from the fit when we held  $n_0$ , the real part of  $n_c$ ,  $R_c$ , and  $R_s$  constant, chose values of the real part of  $n_s$ , and allowed the algorithm to optimize values of the other fitting parameters. The value of  $\chi^2$  has a clear minimum when the real part of  $n_s = 3.0$ .

Previous measurements of the index of refraction of polycrystalline SnS<sub>2</sub> showed  $n \approx 2.92$  at a wavelength of 1  $\mu\text{m}$ .<sup>31</sup> For SnS, the reported index is  $n > 4$  at  $\lambda = 1 \mu\text{m}$ .<sup>34</sup> Our data is thus more consistent with a dense packing of SnS crystallites, which would be expected to yield an index somewhat below 4. Our measured value of the imaginary part of the refractive index is also more consistent with SnS, which has band-gap absorption near  $\lambda = 1 \mu\text{m}$ . By contrast, SnS<sub>2</sub> has an absorption edge in the green or blue part of the visible spectrum and should therefore have lower absorption at 1.064  $\mu\text{m}$ .<sup>31,32</sup> Hence our XRD and light-scattering results are consistent with formation of SnS. The optical absorbance of this material can reasonably be expected to be reduced at longer wavelengths (e.g., 1.5  $\mu\text{m}$ ). Perhaps absorption could additionally be reduced by further thermal processing under controlled atmosphere to remove remaining reactants.

#### IV. CONCLUSION

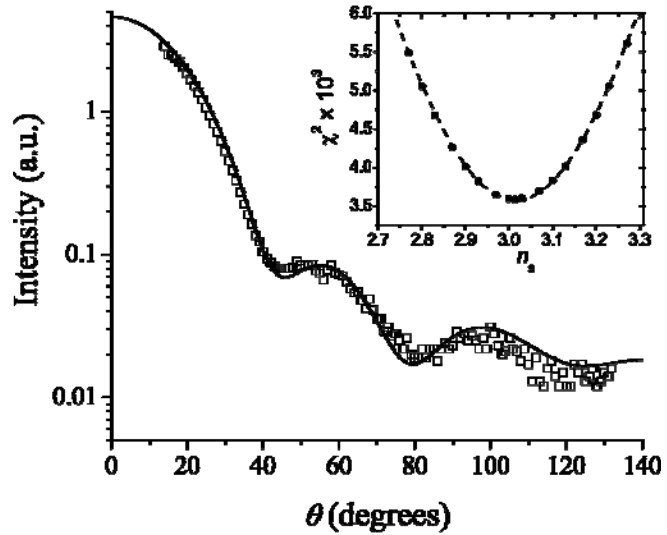


FIG. 5. Plot of the measured intensity as a function of scattering angle,  $\theta$ . The solid curve shows the results of the best fit with an added 1% variation of core size as described in the text. Inset: The values of  $\chi^2$  from the fit, rescaled by  $10^3$ .

In summary, we have presented a straightforward method to prepare colloidal microspheres with a polymeric core and a shell of tin sulfide, most likely SnS. The particles have a narrow distribution of sizes and are stable in suspension, hence able to form ordered arrays. We measured the real part of the refractive index of the shell and found 3.0. To our knowledge, this represents the highest value of refractive index yet attained for smooth colloidal spheres and it may be sufficient to create a complete band gap in the near infrared with a face-centered cubic packing of spheres. Our experiments were done with core particles of polystyrene with diameters of 0.5 to 1.0 microns, but we see no reason why the method cannot be extended to much smaller particles. In addition to their potential application in photonic crystals, these materials might also be useful where strongly-scattering particles are needed as tracers, or for microsphere-based optical resonators.

## ACKNOWLEDGMENTS

We gratefully acknowledge funding by the NSF-supported Materials Research Science and Engineering Center on Polymers at UMass (MRSEC, DMR-0820506). ADD is a Cottrell Scholar of the Research Corporation.

## REFERENCES

1. S. John: Strong Localization of Photons in Certain Disordered Dielectric Superlattices, *Phys. Rev. Lett.* **58**, 2486 (1987).
2. E. Yablonovitch: Inhibited Emission in Solid-State Physics and Electronics, *Phys. Rev. Lett.* **58**, 2059-2062 (1987).
3. S. G. Johnson; J. D. Joannopoulos *Photonic Crystals: the Road from Theory to Practice*; Kluwer Academic Publishers Group: Dordrecht, The Netherlands, 2002.
4. C. Lopez: Materials aspects of photonic crystals, *Adv. Mater.* **15**, 1679 (2003).
5. *Photonic Crystals: Advances in Design, Fabrication, and Characterization*; K. Busch; S. Lolkes; R. B. Wehrspohn; H. Foll, Eds.; Wiley-VCH: Weinheim, 2004.
6. T. Ding; Z. F. Liu; K. Song: Preparation of 3D photonic crystals, *Prog. Chem.* **20**, 1283 (2008).
7. P. V. Braun; S. A. Rinne; F. Garcia-Santamaria: Introducing defects in 3D photonic crystals: State of the art, *Adv. Mater.* **18**, 2665 (2006).
8. G. von Freymann; A. Ledermann; M. Thiel; I. Staude; S. Essig; K. Busch; M. Wegener: Three-Dimensional Nanostructures for Photonics, *Adv. Funct. Mater.* **20**, 1038 (2010).
9. K. M. Ho; C. T. Chan; C. M. Soukoulis: Existence of a Photonic Band Gap in Periodic Dielectric Structures, *Phys. Rev. Lett.* **65**, 3152 (1990).
10. R. Biswas; M. M. Sigalas; G. Subramania; K. M. Ho: Photonic Band Gaps in Colloidal Systems, *Phys. Rev. B* **57**, 3701 (1998).
11. K. Busch; S. John: Photonic Band Gap Formation in Certain Self-Organizing Systems, *Phys. Rev. E* **58**, 3896 (1998).
12. A. Imhof; D. J. Pine: Ordered Macroporous Materials by Emulsion Templating, *Nature* **389**, 948-951 (1997).
13. A. A. Zakhidov; R. H. Baughman; Z. Iqbal; C. Cui; I. Khayrullin; S. O. Dantas; J. Marti; V. G. Ralchenko: Carbon Structure with Three-Dimensional Periodicity at Optical Wavelengths, *Science* **282**, 897 (1998).
14. A. Blanco; E. Chomski; S. Grabtchak; M. Ibisate; S. John; S. W. Leonard; C. Lopez; F. Meseguer; H. Miguez; J. P. Mondia; G. A. Ozin; O. Toader; H. M. van Driel: Large-Scale Synthesis of a Silicon Photonic Crystal with a Complete Three-Dimensional Bandgap near 1.5 Micrometres, *Nature* **405**, 437 (2000).
15. M. Muller; R. Zentel; T. Maka; S. G. Romanov; C. M. S. Torres: Photonic crystal films with high refractive index contrast, *Adv. Mater.* **12**, 1499 (2000).
16. Z.-Q. Zhang; P. Sheng, "Wave Diffusion and Localization in Random Composites," in *Scattering and Localization of Classical Waves in Random Media*; Sheng, P., Ed.; World Scientific: Singapore, 1990; vol.

17. K. Busch; C. M. Soukoulis: Transport Properties of Random Media: A New Effective Medium Theory, *Phys. Rev. Lett.* **75**, 3442 (1995).
18. K. Busch; C. M. Soukoulis: Energy-density CPA: a new effective medium theory for classical waves, *Physica B* **296**, 56 (2001).
19. K. P. Velikov; A. van Blaaderen: Synthesis and characterization of monodisperse core-shell colloidal spheres of zinc sulfide and silica, *Langmuir* **17**, 4779 (2001).
20. M. L. Breen; A. D. Dinsmore; R. H. Pink; S. B. Qadri; B. R. Ratna: Sonochemically produced ZnS-coated polystyrene core-shell particles for use in photonic crystals, *Langmuir* **17**, 903 (2001).
21. J. L. Yin; X. F. Qian; J. Yin; M. W. Shi; G. T. Zhou: Preparation of ZnS/PS microspheres and ZnS hollow shells, *Mater. Lett.* **57**, 3859 (2003).
22. A. Pich; J. Hain; Y. Prots; H. J. Adler: Composite polymeric particles with ZnS shells, *Polymer* **46**, 7931 (2005).
23. T. H. Ji; G. R. Liu; X. Y. Qi; H. B. Xu; M. Y. Gao: Solid-CdS and hollow-ZnS porous submicro spheres: Direct preparation by C-S decomposition of thiol via solvothermal processing, *Mater. Res. Bull.* **42**, 720 (2007).
24. K. J. Huang; P. Rajendran; C. M. Liddell: Chemical bath deposition synthesis of sub-micron ZnS-coated polystyrene, *J. Colloid Interface Sci.* **308**, 112 (2007).
25. D. Son; A. Wolosiuk; P. V. Braun: Double Direct Templated Hollow ZnS Microspheres Formed on Chemically Modified Silica Colloids, *Chem. Mat.* **21**, 628 (2009).
26. C. X. Song; M. L. Yang; D. B. Wang; Z. S. Hu: Synthesis and optical properties of ZnS hollow spheres from single source precursor, *Mater. Res. Bull.* **45**, 1021 (2010).
27. Q. Peng; Y. J. Dong; Y. D. Li: ZnSe semiconductor hollow microspheres, *Angew. Chem.-Int. Edit.* **42**, 3027 (2003).
28. M. Agrawal; S. Gupta; M. Stamm: Recent developments in fabrication and applications of colloid based composite particles, *J. Mater. Chem.* **21**, 615 (2011).
29. M. Agrawal; A. Pich; N. E. Zafeiropoulos; M. Stamm: Fabrication of hollow titania microspheres with tailored shell thickness, *Colloid Polym. Sci.* **286**, 593 (2008).
30. W. H. Suh; A. R. Jang; Y. H. Suh; K. S. Suslick: Porous, hollow, and ball-in-ball metal oxide microspheres: Preparation, endocytosis, and cytotoxicity, *Adv. Mater.* **18**, 1832 (2006).
31. G. Domingo; R. S. Itoga; C. R. Kannewur: Fundamental Optical Absorption in SnS<sub>2</sub> and SnSe<sub>2</sub>, *Phys. Rev.* **143**, 536 (1966).
32. S. Mandalidis; J. A. Kalomiros; K. Kambas; A. N. Anagnostopoulos: Optical investigation of SnS<sub>2</sub> single crystals, *J. Mater. Sci.* **31**, 5975 (1996).
33. M. Deopura; C. K. Ullal; B. Temelkuran; Y. Fink: Dielectric omnidirectional visible reflector, *Opt. Lett.* **26**, 1197 (2001).
34. A. P. Lambros; D. Geraleas; N. A. Economou: Optical-Absorption Edge in SnS, *J. Phys. Chem. Solids* **35**, 537 (1974).
35. J. H. Bang; K. S. Suslick: Applications of Ultrasound to the Synthesis of Nanostructured Materials, *Adv. Mater.* **22**, 1039 (2010).
36. J. Cullity *Elements of X-Ray Diffraction*; Addison-Wesley, 1978.
37. D. Chen; G. Z. Shen; K. B. Tang; S. J. Lei; H. G. Zheng; Y. T. Qian: Microwave-assisted polyol synthesis of nanoscale SnS<sub>x</sub>(x=1,2) flakes, *J. Cryst. Growth* **260**, 469 (2004).
38. A. Sanchez-Juarez; A. Tiburcio-Silver; A. Ortiz: Fabrication of SnS<sub>2</sub>/SnS heterojunction thin film diodes by plasma-enhanced chemical vapor deposition, *Thin Solid Films* **480**, 452 (2005).
39. E. C. Greyson; J. E. Barton; T. W. Odom: Tetrahedral zinc blende tin sulfide nano- and microcrystals, *Small* **2**, 368 (2006).
40. C. Gao; H. L. Shen; L. Sun; Z. Shen: Chemical bath deposition of SnS films with different crystal structures, *Mater. Lett.* **65**, 1413 (2011).
41. J. A. Nelder; R. Mead: A Simplex-Method for Function Minimization, *Comput. J.* **7**, 308 (1965).
42. C. F. Bohren; D. R. Huffman *Absorption and Scattering of Light by Small Particles*; Wiley: New York, 1998.
43. X. Y. Ma; J. Q. Lu; R. S. Brock; K. M. Jacobs; P. Yang; X. H. Hu: Determination of complex refractive index of polystyrene microspheres from 370 to 1610 nm, *Physics in Medicine and Biology* **48**, 4165-4172 (2003).